



Research  
Material Science and Engineering—Article

# Phase Morphology Evolution and Rheological Behavior of Toughened Polypropylene Composite with Controllable Brittle–Ductile Transition Temperature Using SEPS@HDPE Core–Shell Structure

Jiahao Shen<sup>a</sup>, Zhiyi Zhang<sup>a,\*</sup>, Wenwen Yu<sup>a,\*</sup>, Jiayi Wang<sup>a</sup>, Weixuan Wang<sup>a</sup>, Yonggang Shanguan<sup>b</sup>, Qiang Zheng<sup>a,b,\*</sup>

<sup>a</sup> College of Materials Science and Engineering, Taiyuan University of Technology, Taiyuan 030024, China

<sup>b</sup> Department of Polymer Science and Engineering, Zhejiang University, Hangzhou 310027, China

## ARTICLE INFO

### Article history:

Received 7 July 2023

Revised 3 March 2024

Accepted 23 April 2024

Available online 10 December 2024

### Keywords:

Core–shell structure

Low-temperature toughness

Phase morphology evolution

Rheological behavior

## ABSTRACT

The toughness of thermoplastic polymers such as polypropylene (PP) can be improved by adding elastomers-based toughening agents, and the phase morphology of these toughening agents is very important for the strength and toughness of PP. The low-temperature toughness of PP was improved by inserting high-density polyethylene (HDPE) between PP and polystyrene-*b*-ethylene-*co*-propylene-*b*-polystyrene (SEPS) to form an unusual SEPS@HDPE core–shell structure, with SEPS as the core and HDPE as the shell. Based on the microtopography and rheological behavior characterization, HDPE in PP/SEPS/HDPE composites was found to serve as an emulsifier, decrease the size of SEPS particles, and promote the homogeneous dispersion of dispersed phase particles in the matrix. An increase in the HDPE content shifted the toughening mechanism of PP composites from cavitation to matrix shear yielding. The reduction in the distance between the dispersed core–shell structure particles promoted shear yielding in the PP composites, leading to increased toughness. The creation of an intermediate HDPE layer with a moderate modulus was crucial for dispersing stress concentrations and significantly improving toughness without compromising the tensile strength. These findings will facilitate the fabrication of high-toughness PP products at low temperatures.

© 2024 THE AUTHORS. Published by Elsevier LTD on behalf of Chinese Academy of Engineering and Higher Education Press Limited Company. This is an open access article under the CC BY license (<http://creativecommons.org/licenses/by/4.0/>).

## 1. Introduction

Polypropylene (PP) is a commonly used thermoplastic material that exhibits high thermal and chemical resistance, melting point, and hardness, along with low density and reusability. As a typical pseudo-ductile thermoplastic polymer, PP exhibits a yield stress lower than its craze initiation stress and tends toward yielding [1]. While unnotched PP samples are ductile and exhibit shear yielding over a relatively large volume, notched PP is brittle and demonstrates low crack propagation resistance. The sharp notch acts as a stress concentrator, promoting crazing and thus limiting the application scope of the material. The toughness of thermoplastic resins is notably affected by temperature and decreases

when the ambient temperature decreases; this transition is often referred to as the brittle–ductile transition.

The initial temperature at which the change from brittle to ductile occurs is called the brittle–ductile transition temperature ( $T_{bd}$ ) [2]. Pseudo-ductile thermoplastic polymers such as PP exhibit a sharp change in toughness when the ambient temperature varies [1]. Hence, reducing  $T_{bd}$  is crucial for improving the toughness of PP. A standard method for increasing the toughness of thermoplastic polymers involves adding elastomers to form microparticles [3–6].

However, increasing the rubber content increases the toughness of polymer materials, while their strength or modulus are monotonically decreased. One strategy for maintaining a balance among the strength, modulus, and toughness involves the precise control of the phase morphology. Chen et al. [7,8] blended PP with high-density polyethylene (HDPE) and ethylene–propylene rubber (EPR) and obtained a core–shell structure with an HDPE core encapsulated by an EPR shell in the PP matrix. The HDPE core

\* Corresponding authors.

E-mail addresses: [zhangzhiyi@tyut.edu.cn](mailto:zhangzhiyi@tyut.edu.cn) (Z. Zhang), [yuwenwen@tyut.edu.cn](mailto:yuwenwen@tyut.edu.cn) (W. Yu), [zhengqiang@tyut.edu.cn](mailto:zhengqiang@tyut.edu.cn) (Q. Zheng).

increased the effective volume fraction of rubber without increasing the actual rubber content. Dou et al. [9] controlled the morphology of HDPE-grafted maleic anhydride filler/ethylene-propylene–diene rubber/polyamide, forming small HDPE-core rubber and multiple-HDPE-core rubber particles. The composite comprising multiple-HDPE-core rubber had a strong influence on toughness at room temperature, and the performance of the composite which comprised small HDPE-core rubber was acceptable. These hard-core soft-shell structures (HDPE as the core and the elastomer as the shell) can toughen PP; however, the mechanism underlying core–shell structure formation is not clear. To the best of our knowledge, no reports indicate whether other toughened PP composites, which have core–shell structures, such as soft-core hard-shell (the elastomer as the core, HDPE as the shell), can be prepared by blending. Therefore, the investigation of hard shell structure by precisely controlling the phase morphology and exploring its effect on the strength, modulus, and toughness are necessary for comprehensively understanding the regulation and toughening mechanisms of core–shell structure systems.

In this study, we blended PP with HDPE and polystyrene-*b*-ethylene-*co*-propylene-*b*-polystyrene (SEPS) to obtain an unusual SEPS@HDPE core–shell structure with SEPS as the core and HDPE as the shell in PP. The core–shell structure had a low elastomer content, high low-temperature toughness, and low stiffness loss. For clarity, PP/SEPS composite with the fixed mass ratio of 70/30 was denoted as PPM, and HDPE was used as additive to further toughen the PPM. We investigated the temperature dependence,  $T_{bd}$ , and rheological behavior of the composite as well as the evolution of the HDPE-stacked SEPS microparticle morphology. Finally, we established the relationship between the particle morphology and rheological behavior and proposed a possible toughening mechanism for the composite.

## 2. Materials and methods

### 2.1. Materials

All materials used in this study were commercially available. PP (T300; melt mass-flow rate (MFR): 3.0 g per 10 min (International Organization for Standardization (ISO) 1133); isotacticity: >96%; tensile strength: 32.9 MPa; Young's modulus: 1452 MPa; elongation at break: 69%) was purchased from Sinopec Shanghai Petrochemical Co., Ltd., China. SEPS (YH4053; number average molar mass ( $M_n$ ):  $\sim 1.65 \times 10^5$ ; hydrogenation degree:  $\geq 98\%$ ; theoretical styrene content: 30%) was supplied by Baling Petrochemical Co., Ltd., China. HDPE (5000S; MFR: 0.9 g per 10 min) was purchased from Daqing Petrochemical Co., Ltd., China. The antioxidant, Irganox 1010, was purchased from BASF (Germany).

### 2.2. Sample preparation

A one-step preparation method was used, in which PP, SEPS, and HDPE were mixed at 195 °C for 20 min at a stirring speed of 50 r·min<sup>-1</sup> using HAAKE PolyLab QC (Thermo Fisher Scientific Inc., USA). The mass ratio of the PP/SEPS/HDPE composites was denoted as xPPM/yHDPE, where *x* and *y* represent the masses of PPM and HDPE, respectively, as the ratio of the total mass of PPM/HDPE which are indicated in the figures. All composites mentioned in this paper were named according to this rule. For comparison, PP/HDPE and PP/SEPS composites were prepared with mass ratio of PP/HDPE = 80/20 and PP/SEPS = 70/30. To prevent polymer aging, all samples were treated with 2% (in mass ratio) antioxidant Irganox 1010 (pentaerythritol-3-(3,5-di-*tert*-butyl-4-hydroxyphenyl propionate)). Standard specimens for the following mechanical property tests were prepared by using an injection

molding machine (BP-8180-A, Baopin Precision Instrument Co., Ltd., China) at 205 °C, with an injection mold pressure of 5 MPa and dwelling time of 15 s to ensure complete mold cavity filling.

### 2.3. Notched Charpy impact strength test

Before the measurement, samples with a 45° V-shaped notch were stored in an incubator (GDWJS-100C, Shanghai Suying Test Instrument Co., Ltd., China) at a predetermined temperature for 5 h. The notched Charpy impact test was performed according to ISO 179-1:2000 and ISO 179-2:1997 standards using a Charpy impact testing machine (XJJUD-5.5(5), Xiamen Chongda Intelligent Technology Co., Ltd., China). The reported results are the averages of at least five samples.

### 2.4. Tensile properties test

The standard tensile test was conducted on dumbbell-shaped specimens at room temperature (25 °C ± 3 °C), using a computer-controlled universal testing machine (5969, Instron, USA), with a test speed of 50 mm·min<sup>-1</sup> in accordance with ISO 527-1:2012 and ISO 527-2:2012 standards. The reported results are the averages of at least five samples.

### 2.5. Measurement of contact angle

To determine the surface tension of all the composite components, the contact angle between the surface of the polymers and two testing liquids, namely, deionized water and methylene iodide, was measured. Measurements were conducted using a sessile drop analysis system (DSA100, KRÜSS, Germany) with at least five drops (5 mL) of the two liquids used to measure the contact angles. Surface tension was calculated using the Owens–Wendt–Rabel–Kaelble (OWRK) method [10,11].

### 2.6. Scanning electron microscopy

Scanning electron microscopy (SEM) was used to observe the morphology of the dispersed phase, in particular, the distribution of rubber components. To remove the SEPS phase, the sample was first cryogenically fractured in liquid nitrogen, and the cryo-fractured surface was etched in *n*-octane at 50 °C for 4 h. Thereafter, the samples were dried in a vacuum oven at 60 °C for 12 h before being examined with a scanning electron microscope (GeminiSEM 360, ZEISS, Germany) at a working voltage of 5 kV.

### 2.7. Transmission electron microscopy

Transmission electron microscopy (TEM) can further confirm the core–shell microstructure of the dispersed phase. Ultrathin sections, with a thickness of approximately 60 nm, were prepared using an ultramicrotome (EM UC7, Leica Microsystems, Japan) at –100 °C. The slices were observed under a transmission electron microscope (JEM-1230, JEOL, Japan) at an accelerating voltage of 200 kV.

### 2.8. Measurement of rheological properties

A rotary rheometer (ARES-G2, TA Instruments, USA) was used to measure the rheological properties of the composites. Parallel plates with a diameter of 25 mm were used along with a sample having a diameter of 25 mm and thickness of 2 mm. The dynamic rheological properties of the sample were tested by sweeping the amplitude oscillation frequency from 0.01 to 100 rad·s<sup>-1</sup> at 195 °C, with 5% strain. Stress relaxation behavior was also observed at 195 °C.

2.9. Atomic force microscopy

An Asylum Research atomic force microscopy (AFM) system (MFP-3D, Oxford Instruments, UK) was used to investigate the modulus of the interlayers between the dispersion phases and PP matrix by amplitude modulation (AM)–frequency modulation (FM) mode, at a scan rate of 1 Hz and scan size of 3 μm. All AFM operations were conducted under room temperature and ordinary pressure.

2.10. Dynamic mechanical analysis

The dynamic mechanical properties of the composites were obtained in the single cantilever mode using a dynamic mechanical analysis (DMA) analyzer (DMA 242 E, NETZSCH, Germany). The samples were heated from −120 to 50 °C at an oscillation frequency of 1 Hz and a heating rate of 3 °C·min<sup>−1</sup>.

2.11. Monitoring the crack evolution process

The crack initiation and propagation stages were observed via a part-impact test, which was performed with an impact test machine (CEAST 9050, Instron); the specimens were maintained at −10 °C for 5 h. The pendulum was raised at angles of 30°, 50°, and 150° from the vertically fixed specimen and then released to hit the specimen. The propagation of cracks stopped in the interior of the PPM/HDPE specimens.

3. Results and discussion

3.1. Brittle–ductile transformation behavior of PPM/HDPE composites

Fig. 1(a) shows the plots of the impact strength against temperature for the pure PP, PP/HDPE binary, and PPM/HDPE composites

with different HDPE contents. The impact strength of the PP/HDPE composites increases with temperature, similar to that of pure PP, and remains below 6 kJ·m<sup>−2</sup> between 0 and 40 °C. Thus, the addition of HDPE alone did not suffice to improve the toughness of pure PP. When HDPE is added to PP/SEPS, leading to the formation of the PPM/HDPE composites, a significant brittle–ductile transition occurs between −15 and −10 °C. At −10 °C, the impact strength of PPM is 13.6 kJ·m<sup>−2</sup>, which rapidly increases to 49.3 kJ·m<sup>−2</sup> at −5 °C. As shown in Fig. 1(b), the initial  $T_{bd}$  of the PPM/HDPE composites depends on the HDPE content.  $T_{bd}$  decreases with an increasing HDPE content, reaching a minimum upon the addition of 10% HDPE, after which  $T_{bd}$  remains stable. However, a slight decrease in the impact strength of PPM/HDPE at −10 °C is observed when the HDPE content exceeds 15% (composites with 90/10, 85/15, and 80/20 proportions exhibit impact strengths of 38.0, 38.8, and 33.8 kJ·m<sup>−2</sup>, respectively). The composites of PP and SEPS with 10%–20% HDPE exhibit an improvement in impact resistance performance of more than 100% in relation to that of PPM at −10 °C. The reduction in the ductility of the control experimental PP/HDPE binary composites at lower temperatures indicates that this phenomenon is associated with the synergistic effect of both the HDPE and SEPS components in the PPM/HDPE composites, enhancing the impact strength.

As shown in Fig. S1 in Appendix A, DMA was performed to determine the glass transition temperature ( $T_g$ ) of the rubber component. For the PPM and PPM/HDPE composites, two distinct damping peaks appear from low to high temperatures (Fig. S1(b)), which are related to the glass transitions of SEPS and PP, respectively. Notably, the  $T_g$  of SEPS is −60 °C and remains unchanged when the HDPE content changes, indicating a minimal correlation between  $T_{bd}$  and  $T_g$  in this system.

Tensile strength is a crucial mechanical property of the PPM/HDPE composites. In relation to those of pure PP, the yield and tensile strengths of PPM decreased, whereas the elongation

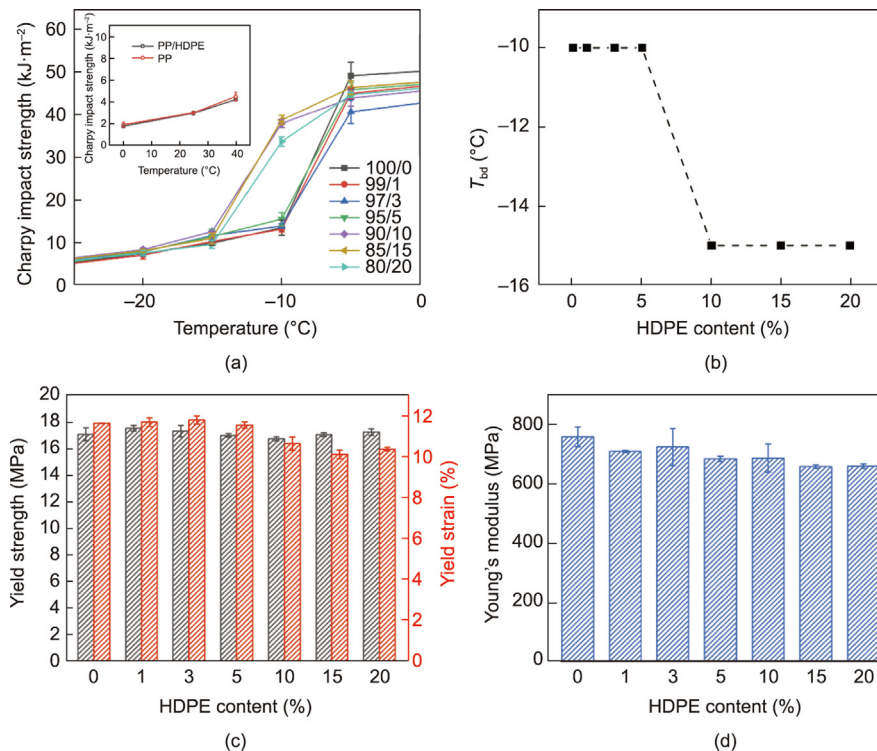


Fig. 1. (a) Plots of notched impact strength versus temperature for the PPM/HDPE composites with different HDPE contents. The inset image provides the plot for the pure PP and PP/HDPE (70/30) samples. (b)  $T_{bd}$  of the PPM/HDPE composites with different HDPE contents. (c, d) Histogram of (c) the yield strength and yield strain, and (d) Young's modulus for PPM and PPM/HDPE composites with different HDPE contents.

at break increased. Fig. S2 in Appendix A illustrates the tensile strength of the PPM/HDPE composites; all PPM/HDPE and PPM composites exhibit excellent mechanical properties, with >500% elongation at break and >25 MPa tensile strength. The tensile yield strength and strain at the yield point were also investigated. Fig. 1(c) illustrates the tensile properties of the PPM/HDPE composites comprising various contents of HDPE. In comparison to that of PPM, the increase in the HDPE content has a minimal impact on the tensile strength, causing only a slight decrease in the yield strain. Therefore, HDPE is an excellent choice for maintaining the strength of PPM. A slight downward trend is observed in the Young's modulus (Fig. 1(d)), corresponding to a reduction in rigidity, possibly owing to a decrease in the PP composition. However, the negligible loss in the Young's modulus is within the acceptable range, considering its effect on the comprehensive mechanical performance. According to the mechanical performance results, the addition of HDPE to PPM can achieve a balance between rigidity and toughness. Other researchers have added rigid fillers to rubber-toughened PP [12–14] or introduced a third phase to form a core-shell structure [8,15] to achieve the desired balance of toughness and strength of the final product. The toughness and strength of rubber-toughened polymer materials are related to the rubber phase and interfacial adhesion between rubber and the polymer matrix [1]. To further explore the underlying mechanism of the aforementioned phenomenon, the rubber phase and interfacial adhesion of PPM/HDPE composites with various HDPE contents were investigated.

### 3.2. Phase morphology evolution of PPM/HDPE composites

Fig. 2 shows the SEM images of the PPM/HDPE composites. Irregular holes are observed because the SEPS particles are etched. Considering that the superficial area of a sphere is the smallest of all spatial geometries when their volumes are equal, the system has a higher interfacial area than spherical systems [12]. The dimensional variations in the phase morphology were calculated using the following methods.

The rubber particle size and size distribution of the PPM/HDPE series as well as the matrix ligament thickness corresponding to the size were analyzed through SEM; the results are shown in Fig. 2. The mean diameter ( $d_w$ ,  $\mu\text{m}$ ) of the elastomer region and matrix ligament thickness (particle spacing,  $l$ ,  $\mu\text{m}$ ) were calculated using the method proposed by Wu [16] and modified by Liu et al. [17] for the analysis of the PPM/HDPE composites.

$$d_w = \frac{\sum_{i=1}^N n_i d_i^2}{\sum_{i=1}^N n_i d_i}$$

$$\ln \sigma = \sqrt{\frac{\sum_{i=1}^N n_i (\ln d_i - \ln d_w)^2}{\sum_{i=1}^N n_i}}$$

$$l = d_w \left[ \left( \frac{\pi}{6\phi} \right)^{\frac{1}{3}} \exp(1.5 \ln^2 \sigma) - \exp(0.5 \ln^2 \sigma) \right]$$
(1)

where  $d_i$ ,  $n_i$ ,  $\phi$ , and  $\sigma$  denote the diameter of the SEPS particle, number of SEPS particles with diameter  $d_i$ , SEPS volume fraction, and diameter distribution of SEPS particles, respectively. To determine the differences, the  $d_w$  and  $l$  values of the composites with specific ratios were used, and the  $d_w$  of the irregular regions was defined by the line connecting the two farthest points. The size of the dispersed phase decreases notably with an increase in the HDPE content. In particular, the addition of 10% HDPE results in the maximal reduction in  $d_w$  of 46% and  $l$  of 76.0%. The particle size distribution coefficient ( $\sigma$ ) also decreases with a reduction in size. Thus, HDPE addition results in finer and denser SEPS microparticle phases. However, the  $l$  values do not decrease further upon the addition of more HDPE because the volume fraction of SEPS in the matrix decreases. Nonetheless, the addition of HDPE refines the size of the dispersed elastomer phase and promotes more uniform phase distribution. Interestingly, the addition of a small amount of HDPE (1%) is effective for toughening PP without significantly changing the phase dispersion, as indicated by the negligible distinctions in  $d_w$ ,  $\sigma$ , and  $l$  between the 100/0 and 99/1 samples, as shown in Fig. 2(a) and Fig. S3 in Appendix A. Additionally, a gradually developing wrinkle is observed at the phase boundary in the highly magnified images, with an increase in the HDPE content from 0% to 20%, indicating that the HDPE content affects the phase interface.

TEM analysis was performed on the ultrathin-sectioned PPM/HDPE composites to further study the phase interface morphology (Fig. 3). SEPS is distributed in PP as dark domains, with polystyrene (PS) segments in SEPS separating as black microphases. The gray regions in Figs. 3(f)–(h) are attributed to HDPE, and have features different from those of the PP matrix. Therefore, the PP, SEPS, and HDPE phase domains are visible in the TEM images. The PPM/HDPE composites exhibit stacked structures when the HDPE content is <10%. As indicated by the circles in Fig. 3(h), the 80/20 samples show complete and clear HDPE shells, while the 90/10

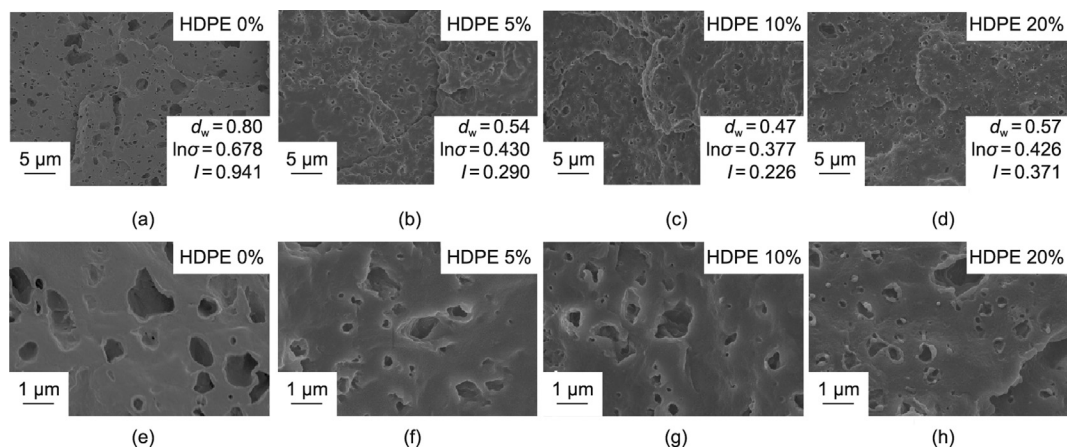


Fig. 2. SEM images of the PPM/HDPE composites with different HDPE contents: (a) 100/0, (b) 95/5, (c) 90/10, and (d) 80/20; and (e–h) are the  $\times 5$  magnification of (a–d).  $d_w$ : mean diameter of the dispersion phase particles ( $\mu\text{m}$ );  $l$ : particle spacing ( $\mu\text{m}$ );  $\sigma$ : the particle size distribution, defined by a log-normal distribution.

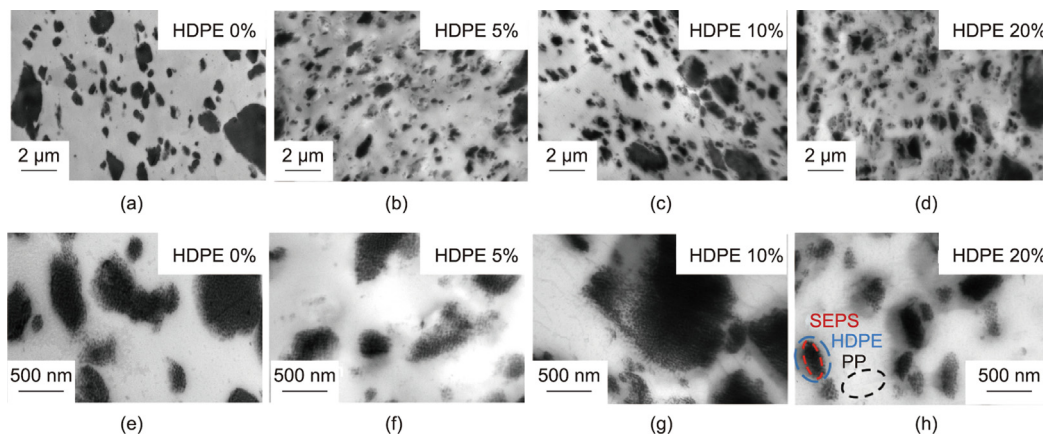


Fig. 3. TEM images of the PPM/HDPE composites with different HDPE contents: (a) 100/0, (b) 95/5, (c) 90/10, and (d) 80/20; and (e–h) are the  $\times 4$  magnification of (a–d).

samples in Fig. 3(g) show thin shells. In previous studies, the appearance of HDPE in PP/EPR increased the size ( $\sim 2 \mu\text{m}$ ) and decreased the particle spacing of the elastomer core-shell structure without increasing the elastomer proportion, leading to improved toughness of PP [6]. In this study, the addition of HDPE to PP/SEPS results in a new core-shell structure with SEPS as the core and HDPE as the shell and the sizes of the SEPS particles decreased to  $< 1 \mu\text{m}$ . Thus, the phase morphology and core-shell structure notably influenced the toughening of PP.

The evolution of the phase structure can be attributed to the spreading coefficient of each component [18–20]. The surface and interfacial tensions were measured to determine the spreading coefficients of the PP/HDPE, PP/SEPS, and HDPE/SEPS composites. The corresponding calculation processes and results are presented in Tables S1 and S2, respectively. The calculated spreading coefficients  $\lambda_{PP}$ ,  $\lambda_{SEPS}$ , and  $\lambda_{HDPE}$  are  $-0.68$ ,  $-0.83$ , and  $-0.17$ , respectively. The specific phase morphologies of the mixtures were predicted based on their spreading coefficients [18]. As illustrated in Fig. S4 in Appendix A, HDPE and SEPS do not induce diffusion between each other and PP. Because PP is not spread between HDPE and SEPS, a stacked microstructure was formed in the PP matrix.

According to the spreading coefficient theory, this stacked microstructure of HDPE and SEPS spreads within the PP matrix [19], which is consistent with the TEM images shown in Figs. 3(b) and (c), provided that the HDPE content does not exceed 10%. However, at the HDPE content of  $> 10\%$ , as in the case of 80/20, SEPS exhibits a dispersed phase morphology wrapped by the HDPE phase, as shown in the TEM images (Fig. 3(d)). The variation in the PPM/HDPE microstructure from a stacked microstructure to a core-shell structure may be attributed to the viscosity ratio because the component with a lower viscosity encapsulates the component with a higher viscosity [21].

The morphological evolution of the dispersed phase is shown in Fig. 4. The addition of HDPE causes a notable decrease in the size of the SEPS particles, which were gradually encapsulated by HDPE. The change in surface energy is associated with the phase morphology and particle size. Low interfacial tension facilitates the formation of a large interfacial area. In a binary composite of two polymers A and B, the third polymer C acts as an emulsifier when the interfacial tension between A and C is lower than that between A and B [22]. The interfacial tension of PP/SEPS and PP/HDPE interfaces are  $0.76$  and  $0.43 \text{ mN}\cdot\text{m}^{-1}$ , respectively. Hence, the experimentally observed decrease in the composite droplet diameter with increasing HDPE concentration can be attributed to a decrease in the interfacial tension between the matrix and dispersed phase due to the encapsulation of SEPS by HDPE. Furthermore, the droplet size of the dispersed phase tends to decrease with decreasing

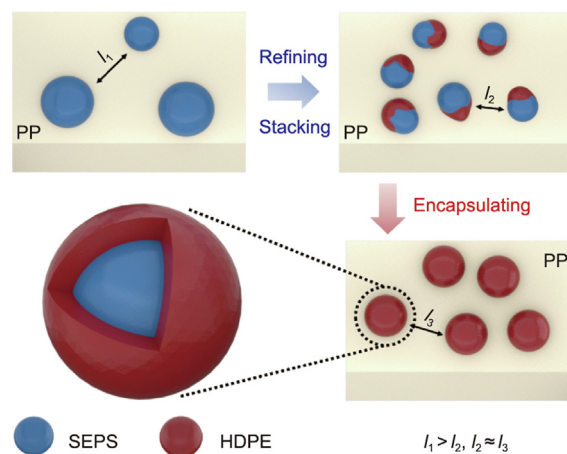
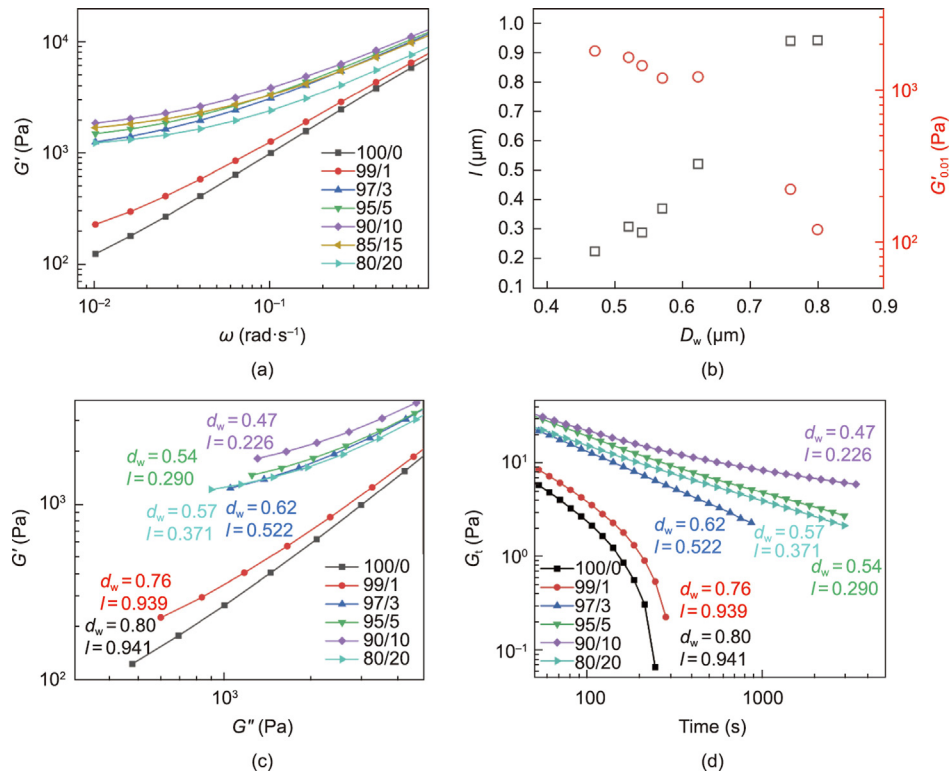


Fig. 4. Schematic of phase evolution and origin of PPM/HDPE toughening with increasing HDPE content.  $l_1$ ,  $l_2$ , and  $l_3$  are particle spacing.

viscosity ratio of the dispersed phase/matrix [23]. Therefore, HDPE, which has a lower viscosity than that of SEPS, can reduce the size of the SEPS phase by lowering the viscosity of the dispersed phase. In the absence of HDPE, the broken SEPS droplets inevitably coalesce under continuous shearing. However, if HDPE is stacked or covers the SEPS phase, coalescence is suppressed, resulting in a significant decrease in the size of the SEPS domains. When the rubber volume fraction is fixed, the decrease in particle size is accompanied by a decrease in particle spacing ( $l_1 > l_2 \approx l_3$ ), resulting in toughening [16].

### 3.3. Rheological behavior of PPM/HDPE composites

Fig. 5(a) illustrates the variation in the dynamic modulus of the PPM/HDPE composites. When the HDPE content is less than 3%, the storage modulus ( $G'$ ) decreases considerably with a decrease in the shear frequency. Fig. 5(b) illustrates the dependence of  $l$  and  $G'_{0.01}$  on  $d_w$ , where  $G'_{0.01}$  denotes the value of storage modulus  $G'$  at low frequencies ( $\omega = 0.01 \text{ rad}\cdot\text{s}^{-1}$ ). In the presence of 3%–20% HDPE, a modulus plateau appears for PP/PPM at low frequencies, indicating a solid-like response [24,25]. The appearance of a secondary modulus plateau at low frequencies is a typical characteristic of solid-particle-filled polymer melts or rubber-modified systems. Additionally, Fig. 5(c) shows the Han plots for PPM and PPM/HDPE. The slope of storage modulus ( $G'$ ) versus loss modulus ( $G''$ ) at low frequencies decreases with the incorporation of HDPE into PPM, and the inflection point shifts to higher frequencies. Regardless of the temperature, any deviation from a slope of 2



**Fig. 5.** (a) Frequency ( $\omega$ ) dependence of storage modulus ( $G'$ ). (b) Correlativity of  $l$ ,  $d_w$ , and  $G'_{0.01}$  ( $\omega = 0.01$  rad·s<sup>-1</sup>). (c) Storage versus loss modulus (Han plots). (d) Stress relaxation behavior of the PPM/HDPE composites with different HDPE contents and with  $d_w$  and  $l$  marked.  $G_t$ : shear relaxation modulus.

indicates microheterogeneity instead of the melting of homogeneous polymer to form solutions [26]. The change in the slope of  $G'$  versus  $G''$  indicates significant microstructural changes in the PPM matrix upon HDPE addition. Similar tendencies are observed in the stress relaxation behaviors (Fig. 5(d)); a relaxation plateau is observed when the HDPE content exceeds 3% and continues to increase until the HDPE content exceeds 10%. This represents the relationship between the microheterogeneity and relaxation behavior, referred to as a long-term relaxation unit.

A skeletal structure forms when the concentration of dispersed domains is sufficiently high to dominate interparticle interactions or the dispersion of aggregates [27,28]. Therefore, investigating the causes for the formation of long-term relaxation units is critical for elucidating the specific role of HDPE in the system.

Based on the correspondence between the particle size and spacing (matrix ligament thickness) of elastomer-toughened PP and the stress relaxation behavior [29], we combined the statistical results of the particle size ( $d_w$ ) and particle spacing ( $l$ ) with the rheological behavior. Our findings indicate that the existence of a percolated network microstructure resulting from an increase in the particle dispersion or a change in the specific surface area [21,24,27] may be the source of the long-term relaxation unit. Because the calculation of  $l$  involves comparable percentages of SEPS, the influence of the difference in the volume fraction can be neglected. Therefore, it is found that a smaller particle size and higher particle density contribute to a closer spacing between the particles in Fig. 5(b). An inverse relationship is observed between  $G'_{0.01}$ ,  $d_w$ , and  $l$ , indicating that a closer spacing of particles leads to long-term relaxation. Furthermore, as illustrated in Figs. 5(c) and (d), a decrease in the slope of  $G'$  versus  $G''$  at low frequencies and an increase in the height of the shear relaxation modulus ( $G_t$ ) platform are correlated with the matrix ligament thickness. These findings indicate that a percolated network

microstructure results in the formation of long-term relaxation units.

A relatively low concentration of HDPE (3%) promotes the formation of physical networks of SEPS particles. However, when the HDPE content exceeds 10%, all relevant parameters across the full frequency range decrease slightly, possibly because of a decrease in the SEPS content accompanied by an increase in the lower-viscosity HDPE content [27], thereby weakening the physical network. As indicated by the TEM images, a fully coated structure appears when the HDPE content exceeds 10%, and the SEPS particle size variation becomes relatively stable. Therefore, the evolution of the core-shell structure is not considered a determining factor for the relaxation behavior.

### 3.4. Toughening mechanism of PPM/HDPE composites

Typically, the impact toughness of polymer materials is influenced by the content, size, and diameter of homogeneous rubber microparticles [1]. The diameter of the composite droplets decreases according to the brittle-ductile transition owing to the transition in the matrix deformation mode from excessively large rubber void-initiated localized crazes to that of fine rubber void-initiated extensive shear yielding [30].

Fig. 6 depicts the topography of the failure surface tested at -10 °C. When the HDPE content is less than 10%, only cavitation is observed in the matrix, corresponding to brittle fracture. At lower temperatures, the toughness of the matrix decreases, and the cavitation of rubber is more likely to form cracks, resulting in brittle failure. However, when the HDPE content reaches 10%, the sample exhibits ductile fracture characteristics and the matrix undergoes continuous shear yielding perpendicular to the impact direction. Similar shear yielding of the matrix is observed in the 80/20 composites. Therefore, unlike the hard-core soft-shell struc-

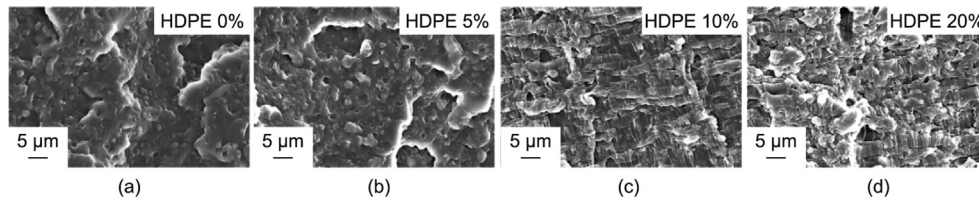


Fig. 6. SEM images of the failure section of the PPM/HDPE composites after the impact test at  $-10\text{ }^{\circ}\text{C}$ : (a) 100/0, (b) 95/5, (c) 90/10, and (d) 80/20.

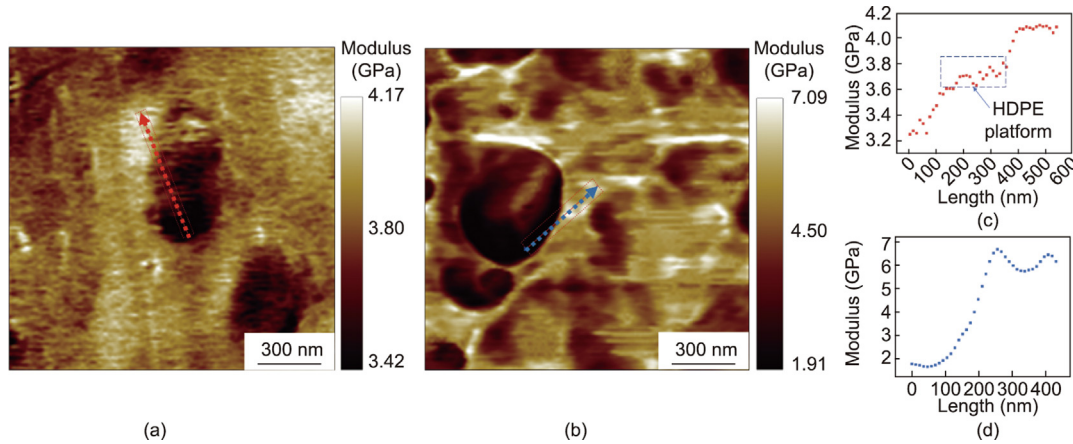


Fig. 7. AFM image analysis of (a) PPM/HDPE (90/10) and (b) PPM, where (c) and (d) represent the modulus distribution on the lines shown in (a) and (b), respectively. The arrows indicate the direction of distance increase.

ture that toughens PP, the toughening mechanism of the PPM/HDPE composites can be attributed to the unusual soft-core hard-shell structure caused by the HDPE-induced transition of the matrix failure source from cavitation to continuous shear yielding.

Although the 95/5 and 80/20 samples contain dispersed phases with similar particle sizes, their impact properties and fracture profiles are dissimilar, indicating that HDPE addition can considerably affect the samples in addition to altering the phase size. Therefore, further investigation of the intermediate HDPE layers is required. Figs. 7(a) and (b) display the images obtained from the AFM analysis of the 90/10 and PPM samples, respectively; the Young’s modulus is shown in Figs. 7(c) and (d). Interestingly, two modulus plateaus are observed at the interface of the PPM/HDPE sample corresponding to the moduli of SEPS, HDPE, and PP, which range from low to high; by contrast, PPM exhibits a single sharp change. Hence, HDPE forms an intermediate layer that induces a moderate modulus that helps disperse stress concentrations [31].

As shown in Fig. 8, the initial crack originates from the tip of the notch, leading to stress whitening, which is indicative of cavitation and plastic deformation. Compared to pure PPM, the PPM/HDPE composites display stress-whitening regions with larger radii. Moreover, the PPM/HDPE composites exhibit smaller crack lengths. In the impact test, with the pendulum raised to an angle of  $150^{\circ}$ , the crack terminates inside the PP/HDPE specimen, whereas the PPM specimen is completely destroyed. These observations confirm that the SEPS@HDPE core-shell structure within the PPM/HDPE composites facilitates the enhanced dispersion of the internal stress. This enhanced stress dispersion promotes a wider range of plastic deformation around the crack tip, and consequently, effectively suppresses the progression of cracks.

We propose a mechanism for enhancing the toughness of the samples at low temperatures using the SEPS@HDPE core-shell structure by adding HDPE. HDPE affects the interface between other materials via its specific surface tension, tending to form a

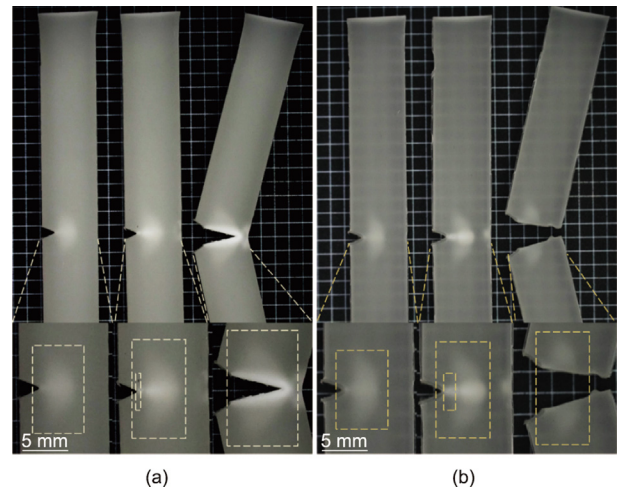


Fig. 8. Crack initiation progress of (a) PPM/HDPE (90/10) and (b) PPM.

large interface area and suppressing SEPS coalescence, thereby considerably reducing the dispersed phase size. Therefore, a larger number and smaller size of the dispersed phases are more likely to result in a wide range of matrix shear yields, which is considered to be the cause of the increased material toughness. Moreover, an HDPE interlayer disperses concentrated stress, further reducing the volume of cavitation holes. Owing to the stronger yield tendency of PP than fracture, the matrix undergoes shear yielding. The decreased size of the dispersed phase and the presence of the HDPE-coated structure cause a notable increase in the impact strength of the PPM/HDPE samples.

#### 4. Conclusions

This study demonstrated that the addition of HDPE to PPM, forming the PPM/HDPE composites with the SEPS@HDPE core-

shell structure, effectively alters  $T_{bd}$  and improves toughness. Also, the PPM/HDPE composites were found to maintain a tensile strength comparable to that of PP/SEPS composites. The evolution of the dispersed phase in the PPM/HDPE composites was explained by the spreading coefficient theory, which posits that a stacked structure of the dispersed phase is observed at low HDPE contents, and a core-shell structure is formed at high HDPE contents. The rheological behavior further confirmed the correlation between the dispersed phase evolution and mechanical properties of the PPM/HDPE composites, and the soft-core hard-shell structure toughened PP. This work also proves that the composition and phase morphology of toughening agents are very important to the strength and toughness of PP composites, and the low-temperature toughening strategy based on soft-core hard-shell mechanism may be used for other thermoplastic polymers.

### Declaration of competing interest

The authors declare that they have no known competing financial interests or personal relationships that could have appeared to influence the work reported in this paper.

### Acknowledgments

This study was supported by the Taiyuan Major Science and Technology Project Fund in 2021, Fund for Shanxi “1331 Project,” Key Research and Development Program of Shanxi Province (202102040201011), and the Zhanjiang Marine Equipment and Marine Biological Industry Unveiled the Talent Team Project (2021E05034).

### Appendix A. Supplementary data

Supplementary data to this article can be found online at <https://doi.org/10.1016/j.eng.2024.04.027>.

### References

- [1] Wang J, Zhang X, Jiang L, Qiao J. Advances in toughened polymer materials by structured rubber particles. *Prog Polym Sci* 2019;98:101160.
- [2] Zhu L, Li M, Zhao S, Bao S, Chen F, Shangguan Y, et al. Ultra-high impact PPR composites at low-temperature through enhanced preferential loading of nanoparticles at polymeric interface induced by properly vulcanized rubber dispersed phase. *Compos Sci Technol* 2022;227:109593.
- [3] Gupta AK, Purwar SN. Dynamic mechanical and impact properties of PP/SEBS blend. *J Appl Polym Sci* 1986;31(2):535–51.
- [4] Karger-Kocsis J, Kuleznev VN. Dynamic mechanical and impact properties of polypropylene/EPDM blends. *Polymer* 1982;23(5):699–705.
- [5] Jia E, Shangguan Y, Xiong J, Chen F, Zheng Q. Fabrication of polypropylene blends with excellent low-temperature toughness and balanced toughness-rigidity by a combination of EPR and SEEPS. *J Appl Polym Sci* 2018;135(3):45714.
- [6] Chen F, Qiu B, Wang B, Shangguan Y, Zheng Q. Balanced toughening and strengthening of ethylene-propylene rubber toughened isotactic polypropylene using a poly(styrene-*b*-ethylene-propylene) diblock copolymer. *RSC Adv* 2015;5(27):20831–7.
- [7] Chen F, Qiu B, Shangguan Y, Song Y, Zheng Q. Correlation between impact properties and phase structure in impact polypropylene copolymer. *Mater Des* 2015;69:56–63.
- [8] Chen F, Shangguan Y, Jiang Y, Qiu B, Luo G, Zheng Q. Toughening with little rigidity loss and mechanism for modified polypropylene by polymer particles with core-shell structure. *Polymer* 2015;65:81–92.
- [9] Dou R, Shen C, Yin B, Yang M, Xie B. Tailoring the impact behavior of polyamide 6 ternary blends via a hierarchical core-shell structure *in situ* formed in melt mixing. *RSC Adv* 2015;5(19):14592–602.
- [10] Owens DK, Wendt RC. Estimation of the surface free energy of polymers. *J Appl Polym Sci* 1969;13(8):1741–7.
- [11] Kaelble DH. Dispersion-polar surface tension properties of organic solids. *J Adhes* 1970;2(2):66–81.
- [12] Jia E, Zhao S, Shangguan Y, Zheng Q. A facile fabrication of polypropylene composites with excellent low-temperature toughness through tuning interfacial area between matrix and rubber dispersion by silica nanoparticles located at the interface. *Compos Sci Technol* 2019;184:107846.
- [13] Zhao S, Shangguan Y, Wu Q, Li Z, Zheng Q. Toughening mechanism of PP/EPR/SiO<sub>2</sub> composites with superior low-temperature toughness. *Compos Sci Technol* 2021;207:108691.
- [14] Zhao S, Hu R, Zhu L, Li M, Chen F, Wu Q, et al. Adjustable brittle-ductile transition behavior and rheological behavior of polypropylene random copolymer nanocomposites through well interfacial-loaded nanoparticles. *Compos Part B* 2022;238:109939.
- [15] Jia E, Zhao S, Shangguan Y, Zheng Q. Toughening mechanism of polypropylene blends with polymer particles in core-shell structure: equivalent rubber content effect related to core-shell interfacial strength. *Polymer* 2019;178:121602.
- [16] Wu S. A generalized criterion for rubber toughening: the critical matrix ligament thickness. *J Appl Polym Sci* 1988;35(2):549–61.
- [17] Liu ZH, Zhang XD, Zhu XG, Qi ZN, Wang FS. Effect of morphology on the brittle ductile transition of polymer blends: 1. a new equation for correlating morphological parameters. *Polymer* 1997;38(21):5267–73.
- [18] Mao Z, Zhang J. Largely improved the low temperature toughness of acrylonitrile-styrene-acrylate (ASA) resin: fabricated a core-shell structure of two elastomers through the differences of interfacial tensions. *Appl Surf Sci* 2018;444:345–54.
- [19] Li H, Xie XM. Morphology development and superior mechanical properties of PP/PAG/SEBS ternary blends compatibilized by using a highly efficient multi-phase compatibilizer. *Polymer* 2017;108:1–10.
- [20] Hobbs SY, Dekkers MEJ, Watkins VH. Effect of interfacial forces on polymer blend morphologies. *Polymer* 1988;29(9):1598–602.
- [21] Nemirovski N, Siegmann A, Narkis M. Morphology of ternary immiscible polymer blends. *J Macromol Sci Part B Phys* 1995;34(4):459–75.
- [22] Valera TS, Morita AT, Demarquette NR. Study of morphologies of PMMA/PP/PS ternary blends. *Macromolecules* 2006;39(7):2663–75.
- [23] Wu S. Formation of dispersed phase in incompatible polymer blends: interfacial and rheological effects. *Polym Eng Sci* 1987;27(5):335–43.
- [24] Galgali G, Ramesh C, Lele A. A rheological study on the kinetics of hybrid formation in polypropylene nanocomposites. *Macromolecules* 2001;34(4):852–8.
- [25] Solomon MJ, Almusallam AS, Seefeldt KF, Somwangthanaroj A, Varadan P. Rheology of polypropylene/clay hybrid materials. *Macromolecules* 2001;34(6):1864–72.
- [26] Han CD, Jhon MS. Correlations of the first normal stress difference with shear stress and of the storage modulus with loss modulus for homopolymers. *J Appl Polym Sci* 1986;32(3):3809–40.
- [27] Lertwimolnun W, Vergnes B. Influence of compatibilizer and processing conditions on the dispersion of nanoclay in a polypropylene matrix. *Polymer* 2005;46(10):3462–71.
- [28] Kamal MR, Khoshkava V. Effect of cellulose nanocrystals (CNC) on rheological and mechanical properties and crystallization behavior of PLA/CNC nanocomposites. *Carbohydr Polym* 2015;123:105–14.
- [29] Li M, Zhu L, Chen F, Wu Q, Shangguan Y, Zheng Q. Rheology study on polypropylene blends with *in situ* core-shell dispersed particles. *Acta Polym Sin* 2022;53(11):1399–408. Chinese.
- [30] Bucknall CB, Paul DR. Notched impact behaviour of polymer blends: part 2: dependence of critical particle size on rubber particle volume fraction. *Polymer* 2013;54(1):320–9.
- [31] Zhang B, Shao X, Tian M, Ning N, Zhang L, Wang W. Mussel-inspired environmentally friendly dipping system for aramid fiber and its interfacial adhesive mechanism with rubber. *Polymer* 2022;238:124414.